ARTICLE

Check for updates

A novel in-frame *GFAP* p.E138_L148del mutation in Type II Alexander disease with atypical phenotypes

You-Ri Kang [ID]1,6, So-Hyun Lee [ID]2,6, Ni-Hsuan Lin3,6, Seung-Jin Lee4,6, Ai-Wen Yang3, Gopalakrishnan Chandrasekaran [ID]2, Kyung Wook Kang1, Mi Sun Jin5, Myeong-Kyu Kim1, Ming-Der Perng [ID]3,7✉, Seok-Yong Choi [ID]2,7✉ and Tai-Seung Nam [ID]1,7✉

Alexander disease (AxD) is a neurodegenerative astrogliopathy caused by mutation in the *glial fibrillary acidic protein* (*GFAP*) gene. A 42-year-old Korean man presented with temporary gait disturbance and psychiatric regression after a minor head trauma in the absence of bulbar symptoms and signs. Magnetic resonance images of the brain and spinal cord showed significant atrophy of the medulla oblongata and the entire spinal cord as well as contrast-enhanced T2 hypointensity in the basal ganglia. DNA sequencing revealed a novel 33-bp in-frame deletion mutation (p.Glu138_Leu148del) within the 1B rod domain of GFAP, which was predicted to be deleterious by PROVEAN analysis. To test whether the deletion mutant is disease-causing, we performed in vitro GFAP assembly and sedimentation assays, and GFAP aggregation assays in human adrenal carcinoma SW13 (Vim⁻) cells and rat primary astrocytes. All the assays revealed that GFAP p.Glu138_Leu148del is aggregation prone. Based on these findings, we diagnosed the patient with Type II AxD. This is a report that demonstrates the pathogenicity of InDel mutation of GFAP through functional studies. This patient's atypical presentation as well as the discrepancy between clinical symptoms and radiologic findings may extend the scope of AxD.

INTRODUCTION

Alexander disease (AxD; Online Mendelian Inheritance in Man (OMIM), #203450) is a rare neurodegenerative astrogliopathy caused by mutation of the *glial fibrillary acidic protein* (*GFAP*) gene [1–3]. The human GFAP is 432-amino acid long and consists of an N-terminal head domain, an α-helical central rod domain including 1 A, 1B, and 2 segments, and a C-terminal tail domain [4–6]. Although heterozygous missense variants account for over 95% of the mutations found in patients with AxD, a small number of in-frame insertion or deletion (InDel) mutations has been also reported (Table 1) [7].

Since 1976, AxD has been traditionally divided into infantile-onset, juvenile-onset, and adult-onset according to the age at onset of symptoms [8]. A revised classification system was proposed in 2011 by Prust and colleagues: Type I may often develop at an earlier age and present with classic cerebral symptoms along with the magnetic resonance imaging (MRI) findings proposed by van der Knaap and colleagues including extensive cerebral white matter abnormalities with a frontal preponderance [9], whereas Type II may develop throughout the lifespan and present with bulbar symptoms, autonomic dysfunction, and ocular movement abnormality with MRI features distinct from Type I, including atrophy of the medulla oblongata and cervical spinal cord [10]. In patients with AxD,

analyzing phenotypic characteristics and their relationship with *GFAP* mutation may be helpful to understand the natural course and pathogenesis of the disease. Despite some reports that the affected amino acids may influence the occurrence of a specific phenotype [7, 11–13], the correlation between the genotype and phenotype of AxD seems to be vague in general [13–15].

In a patient presenting with gait disturbance and psychiatric regression after a minor head trauma, we found severe atrophy of the medulla oblongata (MO) on brain MR images and an in-frame deletion mutation in the 1B rod domain of GFAP (c.413_445delAGGTTGAGAGGGACAATCTGGCACAGGACCT-GG, p.E138_L148del). We then set out to test whether GFAP p.E138_L148del elicits GFAP aggregation, thereby being associated with AxD.

MATERIALS AND METHODS
Subjects and ethics
A 42-year-old Korean male with post-traumatic neuropsychiatric symptoms was studied. Written informed consent for publication of his medical records, MR images and genetic study results was obtained from the patient. This study protocol was approved by the Institutional Review Board at Chonnam National University Hospital (CNUH-2020-018), and was conducted in accordance with the Helsinki Declaration of 1975.

1Department of Neurology, Chonnam National University Medical School and Chonnam National University Hospital, Gwangju 61469, Republic of Korea. 2Department of Biomedical Sciences, Chonnam National University Medical School, Hwasun 58128, Republic of Korea. 3Institute of Molecular Medicine, College of Life Sciences, National Tsing Hua University, Hsinchu 30013, Taiwan. 4Department of Radiology, Chonnam National University Hospital, Gwangju 61469, Republic of Korea. 5School of Life Sciences, Gwangju Institute of Science and Technology, Gwangju 61005, Republic of Korea. 6These authors contributed equally: You-Ri Kang, So-Hyun Lee, Ni-Hsuan Lin, Seung-Jin Lee. 7These authors jointly supervised this work: Ming-Der Perng, Seok-Yong Choi, Tai-Seung Nam. ✉email: mdperng@life.nthu.edu.tw; zebrafish@chonnam.ac.kr; nts0022@hanmail.net

Table 1. Clinical information of AxD cases with in-frame InDel mutations of *GFAP*.

No.	Genetic information				Clinical manifestation										Radiologic manifestation				Ref
	Exon	Domain	Codon change	PROVEAN score	Prust	Russo	AAO (Yr)	AAE (Yr)	Bulba	Motor	Urina	Sleep	Scoli	Psych	SPWM	BG	BS	SC	
1	1	1 A	p.K86_V87delinsEF	−7.876	II	J	7	ND	+	+	+	ND	+	−	+	−	+	ND	29
2	1	1B	p.R124_L125insQLR	−8.534	II	A	32	32	+	+	ND	+	ND	+	+	+	+	+	28
3	1	1B	p.R124_L125insE	−7.264	II	A	46	47	+	+	−	−	ND	ND	ND	ND	+	+	13
4	1	1B	p.R126_L127insRL	−7.262	II	J	9	ND	+	+	+	ND	+	−	+	−	+	+	29
5	1	1B	p.R126_L127insRL	−7.262	II	A	22	27	+	+	−	−	ND	ND	ND	ND	+	+	13
6	1	1B	p.R126_L127insRL	−7.262	II	A	16	20	−	+	+	+	+	−	+	−	+	+	23
7*	1	1B	p.E138_L148del	−51.950	II	UD	<20	42	−	+	+	+	+	+	+	+	+	+	*
8	3	1B	p.R201del	−11.288	II	A	71	71	+	+	+	ND	ND	−	ND	ND	+	ND	30
9	Int.3	1B	p.E207del	−12.417	II	A	ND	76	−	+	−	ND	ND	−	+	−	+	+	31
10	Int.3	1B, 2 A, 2B	p.E207_K260del†	−226.745	II	A	<14	39	+	+	+	ND	ND	−	ND	ND	+‡	+‡	32
11	4	2 A	p.E243dup	−8.684	II	A	22	27	+	+	ND	ND	ND	−	+	−	+	+	33
12	Int.4	2B	p.F261_T302del	−176.938	II	A	38	54	+	+	−	+	ND	−	+	−	+	+	34
13§	5	2B	p.F261_T302del	−176.938	Type I	I	1.5	1.5	−	−	−	ND	ND	ND	+	+	ND	ND	35
14§	5	2B	p.F261_T302del	−176.938	Type I	I	2.9	2.9	−	−	−	ND	ND	ND	+	+	ND	ND	35
15||	5	2B	p.R270_A272del	−19.338	Type I	I	0.25	ND	ND	+	ND	ND	ND	−	ND	ND	ND	ND	36
16	6	2B	p.E332del	−10.638	II	J	7	8	−	+	−	ND	ND	−	+	+	+	−	37
17||	6	2B	p.Y349_Q350insHL	−10.078	Type I	I	0.08	ND	+	ND	ND	ND	ND	ND	ND	ND	ND	ND	9

Prust Prust classification for Alexander disease (AxD); Russo Russo classification for AxD; *AAO* Age at onset; *AAE* Age at examination; Bulba Bulbar symptoms including dysarthria, dysphagia, dysphonia, or palatal tremor; Motor Motor symptoms including gait unsteadiness, weakness of limbs, ataxia, hyperreflexia, and spasticity; Urina Urinary symptoms including frequency, urgency, or incontinence; Sleep Sleep disturbance; Scoli scoliosis; Psych psychomotor symptoms regardless of cognitive function; SPWM abnormality of supratentorial periventricular white matter; BG abnormality of basal ganglia; BS abnormality of brainstem; SC abnormality of spinal cord; Ref reference; I infantile-onset AxD; J juvenile-onset AxD; A adult-onset AxD; Int Intron; ND not described; UD undetermined; *current case; †deletion of the whole of exon 4 including the last 8 amino acids of coil 1B, all amino acids of coil 2 A, and a part of coil 2B; ‡autopsy revealed atrophy of the medulla and all levels of the spinal cord; §patients 13 and 14 are twins; ||, patients 15 and 17 were described to have typical radiologic features consistent with the diagnostic criteria for AxD proposed by van der Knaap with no detailed clinical information.

General reagents

All the chemical reagents and materials used in this study were of analytical grade and purchased from Sigma-Aldrich (St. Louis, MO, USA) unless otherwise specified.

DNA sequencing, DNA manipulation, expression and purification of recombinant GFAPs, in vitro assembly and sedimentation assay, cell culture and transfection, lentivirus production and cell transduction, cell fractionation, western blotting (WB), immunocytochemistry analysis, zebrafish study, electron microscopy study and statistical analysis

Detailed information is provided in the Supplementary Methods.

RESULTS

Clinical findings

A 42-year-old man presented with a month-long history of gait disturbance and right forearm pain. While riding a bicycle, the patient lost his balance and hit his head and right forearm on the road. He experienced temporary pain at the injury sites, but no loss of consciousness, fracture, or intracranial hemorrhage occurred. He had no siblings and was married with no children. He had been taking mood stabilizers for a year under the diagnosis of bipolar disorder and was on medication for nocturia for several years. A neurologic examination showed generalized hyperreflexia, ankle clonus, and positive Hoffman's reflexes and Babinski sign of both sides without muscle weakness. Bulbar symptoms or signs including dysarthria, dysphagia, dysphonia and palatal myoclonus were absent. Neither cerebellar ataxia nor nystagmus was observed. MRI of the patient's brain suggested syringomyelia or myelopathy at the level of cervicomedullary junction of uncertain etiology (Fig. 1a). A total of 2 months after the bicycle accident, his gait became so stiff and spastic that he walked like a person with Parkinsonism. His gait disturbance aggravated such that he was unable to walk independently. Accompanied by the gait disturbance were psychomotor regression, depression, anxiety, shortness of breath, and sleep apnea. However, his neuropsychiatric symptoms improved gradually upon physical rehabilitation and supportive psychotherapy in several months, and his physical and mental state returned to the pre-traumatic condition.

Although he denied gait unsteadiness before the accident, the following findings pointed to chronic inherited neurological disorders including AxD, familial amyotrophic lateral sclerosis (ALS), or spinal muscular atrophy (SMA) of adult-onset: (1) his deceased father developed chronic gait disturbance starting approximately at the age of 40, at which point his father's spine MRI exhibited atrophy of the entire spinal cord (SC), (2) his relatives had noted his odd gait since his early childhood, and (3) according to his colleagues, he had experienced alternating bouts of mania and depression since his mid-twenties.

MRI of the brain and SC showed medullocervical T2-hyperinensity, tadpole-like appearance of the brainstem, upward bowing of the corpus callosum (Fig. 1a), pial fluid-attenuated inversion recovery (FLAIR) signal abnormality in the brainstem and cerebellum (Fig. 1b–e), mild ventriculomegaly, T2-hyperintensity of periventricular WM and basal ganglia (BG) with contrast-enhancement (Fig. 1g–i), thoracic scoliosis and atrophy of the cervical and thoracic SC (Fig. 1j). The ratios of the diameter of MO (7.62 mm) to that of midbrain and pons were 0.51 and 0.35, respectively (figure not shown), which fulfilled the radiologic criteria for the diagnosis of adult-onset Alexander disease proposed by Yoshida and colleagues [16]. Nerve conduction study and electromyography were unremarkable, which excluded familial ALS and SMA.

Mutational analysis

Whole exome sequencing uncovered a novel heterozygous in-frame deletion (p.Glu138_Leu148del) in exon 1 of *GFAP*, and two heterozygous single nucleotide variants (c.1258-86 C>T, rs11651396 and c.1171+459 A>G, rs9916491) in the intronic regions. No mutation was found in the causative genes of several other leukodystrophies, including adrenomyeloneuropathy/X-linked adrenoleukodystrophy (*ABCD1*), Krabbe disease (*GALC*), metachromatic leukodystrophy (*ARSA* & *PSAP*) and Pelizaeus–Merzbacher disease (*PLP1*). Further, no causative mutations were noted in the genes associated with hereditary spastic paraplegia (HSP; 80 *spastic paraplegia genes* [*SPG*]) [17] and familial ALS (*C9ORF72*, *SOD1*, *TARDBP*, *FUS*, *FIG4*, and *ANG*). GAA repeat expansion analyses revealed no expansion, thereby excluding Friedreich ataxia.

Sanger sequencing of *GFAP* uncovered a novel heterozygous in-frame deletion of 33 bp (c.413_445delAGGTTGAGAGGGA-CAATCTGGCACAGGACCTGG, p.E138_L148del, Fig. 1k) at the end of exon 1, which is located in the 1B rod domain (Fig. 1l). This deletion is predicted to remove 11 amino acids (EVERDNLAQDL) from the WT GFAP protein. This mutation was found in neither 200 normal Korean control subjects nor the Exome Variant Server database (http://evs.gs.washington.edu). In contrast to PolyPhen-2 and SIFT, PROVEAN (Protein Variation Effect Analyzer) can predict functional effects of InDel mutations [18]. PROVEAN predicted that the mutation would be deleterious (score: −51.950; cutoff: −2.5).

p.E138_L148del mutation does not reduce the stability of GFAP in HEK293T cells

To check whether the p.E138_L148del mutation suppresses the stability of GFAP protein, we first transfected HEK293T cells, which do not express endogenous GFAP, with plasmids encoding WT GFAP or GFAP p.E138_L148del C-terminally fused to FLAG epitope. As expected, western blotting with anti-FLAG antibody showed that the molecular weight (MW) of GFAP p.E138_L148del is slightly smaller than that of WT GFAP. However, we did not observe any noticeable decrease in expression levels of GFAP p.E138_L148del compared to WT GFAP, indicating that this deletion mutation does not reduce GFAP protein stability. Of note, more mutant GFAP was found in the insoluble fraction (pellet) than WT GFAP (Fig. 1m), suggestive of the aggregation prone nature of GFAP p.E138_L148del. In addition, more WT GFAP was observed in the pellet fraction in the presence of the mutant form, indicating interaction between the mutant and WT GFAPs.

p.E138_L148del aggregates GFAP in vitro

To investigate whether p.E138_L148del is prone to aggregation, we performed in vitro filament assembly studies. While WT GFAP assembled into typical 10-nm intermediate filaments (IFs) that were several microns in length, the deletion mutant failed to form extended filaments. Instead, it formed short filament-like structures that had a strong tendency to laterally associate into aggregates. Because the deletion mutation was heterozygous in the patient, we also examined the assembly behavior of the deletion mutant in the presence of WT GFAP in a 1:1 ratio, and observed aggregates similar to those formed by the mutant alone (Fig. 2). To assess the extent of GFAP aggregation, we first performed a low-speed sedimentation assay. While most of the WT GFAP (>80%) was found in the supernatant fraction, nearly all of the mutant sedimented into the pellet fraction (Fig. 2b, upper panel). Mixture of the mutant and the WT GFAP in a 1:1 ratio yielded higher GFAP levels in the pellet fraction than WT GFAP alone (Fig. 2b, upper panel). High-speed sedimentation revealed that the WT and mutant GFAP, either individually or in combination, were present primarily (>90%) in the pellet fraction, suggesting that they all assembled efficiently (Fig. 2b, lower panel). Collectively, this outcome indicates that the mutant GFAP sediments more efficiently than the WT GFAP, and this effect is dominant over the WT GFAP.
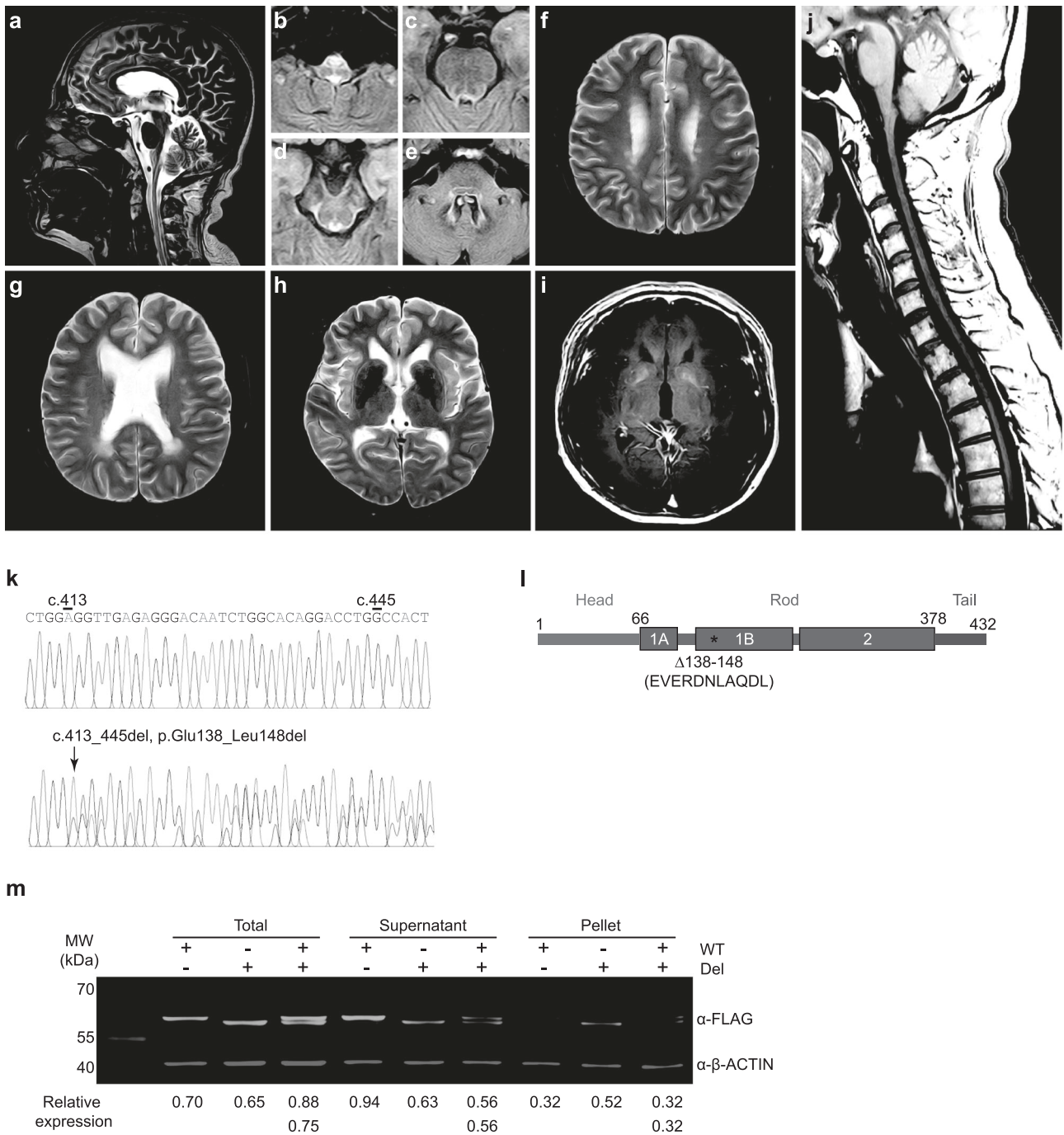
Fig. 1 Radiological and genetic profiles of the proband. a A sagittal T2-weighted brain MR image shows thinning of the corpus callosum, atrophy, and signal changes in the medulla oblongata. **b–e** Axial FLAIR images show the atrophy and abnormal hyperintensity of medulla oblongata, which indicates an "eye spot of Taenaris" sign (**b**), hyperintensity of the peripheral rim of pons (**c**) and midbrain (**d**), and bilateral hyperintense lesions involving the hilum of the dentate nuclei (**e**). **f–h** Axial T2-weighted images show periventricular garlands-like thin bands of signal intensity (**f**), ventriculomegaly (Evans' ratio = 0.38) and bilateral WM hyperintensity of lateral ventricle with posterior predominancy (**g**), and hyperintense putaminal rim sign (**h**). **i** A gadolinium-enhanced axial T1-weighted image shows patchy enhancement in bilateral basal ganglia. **j** A sagittal T1-weighted spine MR image shows atrophy extending from the upper cervical spinal cord to the level of middle thoracic vertebrae. **k** DNA sequence analysis of the WT (upper) and mutant (lower) GFAP. **l** Schematic illustration of human GFAP. The numbers of amino acid residues are based on NP_002046 (NCBI accession number). Asterisk indicates the p.Glu138_Leu148del mutation. Not drawn to scale. **m** Expression levels are comparable in HEK 293 T cells between WT GFAP and GFAP p.Glu138_Leu148del. HEK293T cells were transfected with plasmid encoding WT GFAP, GFAP p.Glu138_Leu148del, or both in a 1:1 ratio, and lysed with RIPA lysis buffer. The resulting lysates were separated into supernatant and pellet fractions and then processed for immunoblotting with anti-FLAG antibody. β-Actin was used as loading control. Numbers at the bottom are intensity of the WT or mutant GFAP protein normalized to that of actin. In lanes with two bands, upper number at the bottom is for mutant GFAP and lower number for WT GFAP. MW, molecular weight.
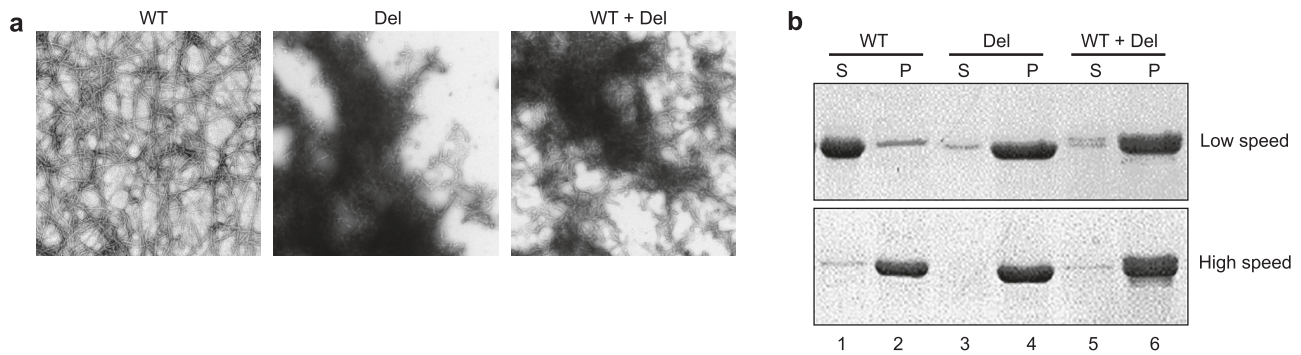
Fig. 2 **GFAP p.E138_L148del is prone to aggregation in vitro. a** Recombinant WT GFAP and GFAP p.E138_L148del (Del) were purified from *E. coli*, assembled in vitro alone or in combination in a 1:1 ratio, negative-stained with uranyl acetate and then imaged via electron microscopy. **b** The assembled GFAPs were subjected to low- and high-speed centrifugation, and the resulting supernatant (S) and pellet (P) fractions were visualized with SDS-PAGE and Coomassie Brilliant Blue staining.

p.E138_L148del aggregates GFAP in human adrenal cortex carcinoma SW13 (Vim⁻) cells and rat primary astrocytes

To assess the ability of the deletion mutant to assemble into the *de novo* IF network, lentivirus expressing WT and mutant GFAPs, either individually or in combination, were transduced into SW13 (Vim⁻) cells that do not express any endogenous cytoplasmic IFs. When expressed in SW13 (Vim⁻) cells, the WT GFAP formed filaments that tend to bundle in most of the transduced cells. In contrast, the deletion mutant failed to assemble into extended filament networks, yet instead formed an irregular pattern of small clumps scattered throughout the cytoplasm. Since the patient was heterozygous for the GFAP deletion, the presence of both WT and deletion mutant GFAP was also tested. Co-transduction of SW13 (Vim⁻) cells with the deletion mutant and WT GFAP in a 1:1 ratio produced GFAP aggregates similar to those formed by the deletion mutant alone, with an additional feature that aggregates appeared to accumulate at the perinuclear regions (Fig. 3a, arrowheads). Presence of WT GFAP failed to rescue the defect in GFAP network formation, suggesting a dominant effect of the deletion mutation. Subsequently, we sought to assess the relative expression levels and solubility of WT and mutant GFAP in SW13 (Vim⁻) cells. To this end, proteins were extracted from the transduced SW13 (Vim⁻) cells using a deoxycholate-based extraction protocol, which solubilizes GFAP filaments while retaining GFAP aggregates [19], and processed for western blotting. The WT and mutant GFAP were expressed at comparable levels. Because of the lack of 11 amino acids, however, the deletion mutant (Fig. 3b, lane 2) had slightly higher electrophoretic mobility than the WT GFAP (Fig. 3b, lane 1). These findings indicate that it is the mutation per se, rather than elevated expression levels, that aggregates mutant GFAP. Analysis of both the supernatant and pellet fractions revealed that while WT GFAP was detected primarily in the supernatant fraction (about 80%; Fig. 3b, lane 4, 3c), approximately 60% of the mutant GFAP was found in the pellet fraction (Fig. 3b, lane 8, 3c), consistent with its sequestration into cytoplasmic aggregates. Co-transduction with lentivirus expressing WT and mutant GFAP in a 1:1 ratio resulted in the partition pattern (Fig. 3b, lanes 6 and 9, 3c) similar to that obtained with mutant transduction alone (Fig. 3b, lanes 5 and 8, 3c). Collectively, these data suggest that the deletion mutant has a dominant effect over the WT GFAP with respect to network formation and filament solubility.

To validate the aforementioned findings in more relevant settings, we repeated the lentivirus transduction in rat primary astrocytes where endogenous GFAP is present. Transduced cells were distinguished from untransduced cells by staining cells with the monoclonal antibody SMI-21, which specifically recognizes human GFAP [20]. When expressed in rat primary astrocytes, the WT GFAP assembled into filamentous networks in most of the transduced cells, whereas the deletion mutant formed large aggregates in almost all transduced cells. These aggregates also disrupted the endogenous GFAP IF networks, causing them to collapse into a large perinuclear aggregate. Co-transduction with the deletion mutant and the WT GFAP in a 1:1 ratio failed to restore IF network formation, and aggregates similar to those from mutant transduction alone were noted (Fig. 3d). To evaluate the solubility of mutant GFAP aggregates, we extracted proteins from the transduced cells and observed that expression levels were comparable between the WT GFAP and mutant (Fig. 3e). However, approximately 85% of the WT GFAPs were extracted into the supernatant fraction (Fig. 3f, lane 1, 3 g), whereas about 70% of mutant GFAP remained in the pellet fraction (Fig. 3f, lane 5, 3 g). Co-transduction with WT GFAP and mutant GFAP in a 1:1 ratio displayed that the pellet fraction (Fig. 3f, lane 6, 3 g) again had higher levels of GFAP than that from cells transduced with WT GFAP alone (Fig. 3f, lane 4, 3 g), suggesting that presence of WT GFAP may not increase the solubility of mutant GFAP. Of note, 53% and 47% of GFAP were observed in the supernatant and pellet fractions, respectively, in the double transduced cells, which is not statistically significantly different from the calculated values (57.5% in the supernatant and 42.5% in the pellet, Fig. 3g). This may be caused by disruption of potential interaction between WT GFAP and mutant GFAP during the protein extraction from the cells. Collectively, these data suggest the dominant effect of the deletion mutant over the WT protein.

DISCUSSION

Here, we show that a 42-year-old Korean man with significant atrophy of the MO and the entire SC on MRI harbors a 33-bp in-frame deletion mutation in *GFAP*, leading to deletion of part of the 1B rod domain. Moreover, we demonstrate that this deletion promotes GFAP aggregation in an in vitro system, SW13 (Vim⁻) cells, rat primary astrocytes and zebrafish. The patient with post-traumatic neuropsychiatric dysfunction is finally diagnosed with Type II AxD.

This case has several characteristics that are not common in AxD. From a clinical perspective, a minor head trauma exacerbated the patient's neuropsychiatric symptoms, but the patient stabilized back to the pre-traumatic state within a few months. This temporary worsening and remission may not be consistent with previously reported AxD cases in which the symptoms worsened steadily after head trauma [21, 22]. In addition, based on his acquaintances' account, it is likely that his symptoms had already existed since his early childhood, which compounded the determination of disease onset. The patient had no bulbar symptoms or signs throughout his life despite significant atrophy and signal change in the MO and brainstem, and even during his post-traumatic neurological deterioration. From a radiological perspective, the patient's MRI revealed T2-hyperintensity of BG with contrast-enhancement and atrophy of the thoracic SC. The former has been reported to be more common in Type I AxD [10],
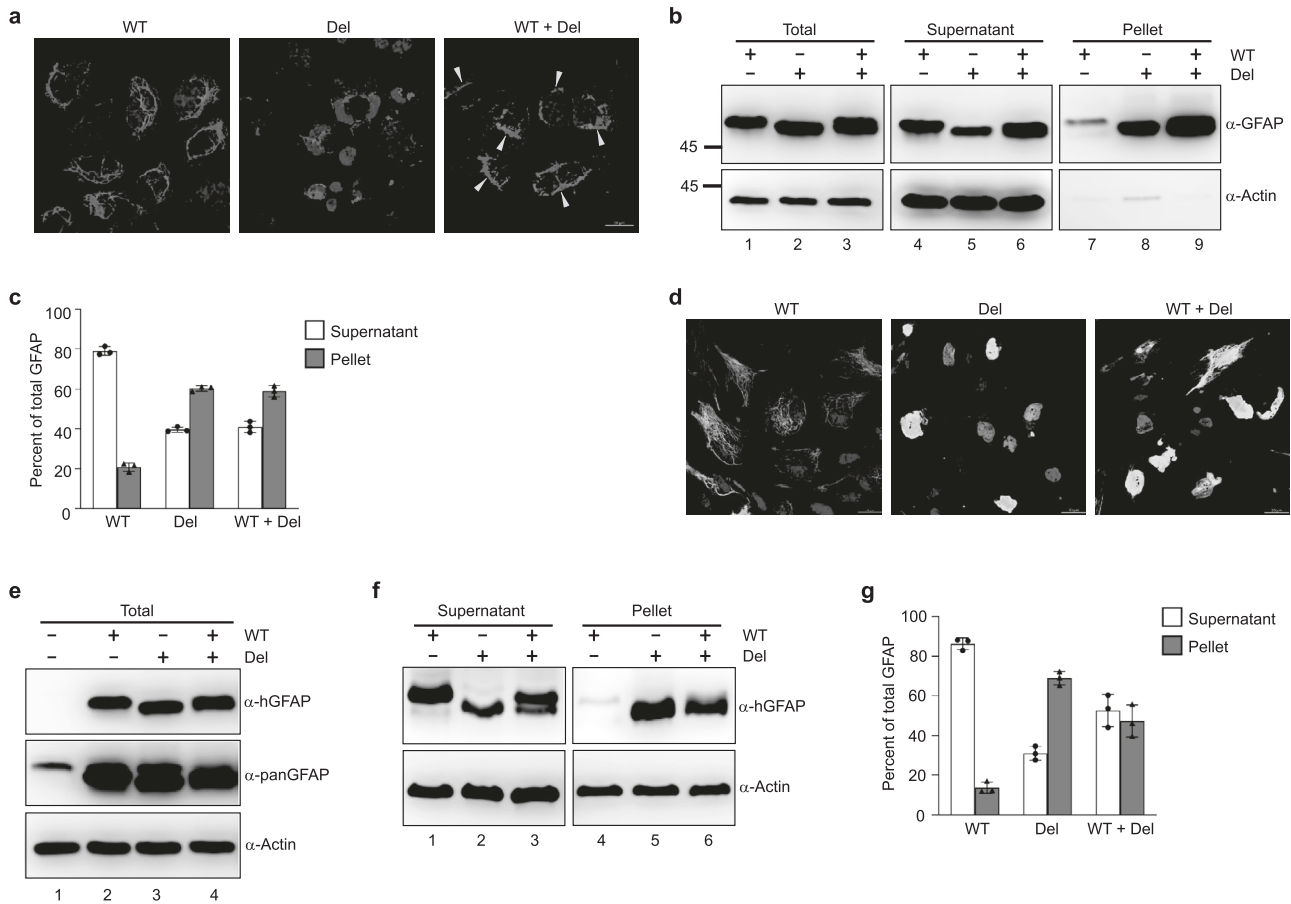
Fig. 3 p.E138_L148del mutation aggregates GFAP in human adrenal cortex carcinoma SW13 (Vim⁻) cells and rat primary astrocytes. a SW13 (Vim⁻) cells were transduced with lentivirus expressing WT GFAP, GFAP p.E138_L148del (Del), or in combination in a 1:1 ratio. At 72 h after transduction, cells were fixed, immunostained with anti-GFAP antibodies (red), counter-stained with DAPI (blue) to visualize nuclei, and imaged using a confocal laser microscope. Arrowheads indicate perinuclear aggregates. Scale bar = 20 μm. **b** The SW13 (Vim⁻) cells in (**a**) were separated into supernatant and pellet fractions, and then processed for immunoblotting with anti-GFAP antibody. Actin was used as loading control. Numbers to the left are molecular weight of protein standards in kDa. **c** Levels of GFAP in (**b**) were quantified ($n = 3$). **d** Rat primary astrocytes were transduced with lentivirus expressing WT GFAP, GFAP p.E138_L148del, or in combination in a 1:1 ratio. At 72 h after transduction, cells were fixed, immunostained with anti-human GFAP (green) and anti-panGFAP (red) antibodies, counter-stained with DAPI (blue), and imaged with a confocal laser microscope. Scale bar = 20 μm. **e**, **f** The rat primary astrocytes in (**c**) were separated into supernatant and pellet fractions, and processed for immunoblotting with anti-human GFAP and anti-panGFAP antibodies. Anti-actin antibody was used as loading control. Cells transduced with empty lentiviral vector were used as negative control (lane 1 in (**d**)). **g** Levels of GFAP in (**f**) were quantified ($n = 3$).

whereas the latter in Type II AxD [23, 24]. From a genetic perspective, the patient harbored an in-frame 33-bp deletion in the 1B rod domain of GFAP, which is an unprecedently large in-frame deletion in the 1B rod domain (Table 1).

AxD can be diagnosed without pathological confirmation (such as Rosenthal fibers) in individuals with typical clinicoradiologic features and a previously reported pathogenic mutation in *GFAP* [7]. The recent advances in DNA sequencing and bioinformatics increase the likelihood of discovering novel *GFAP* variants even in presymptomatic individuals and patients with atypical phenotype [7, 25–27]. However, genome-wide analysis of 60,706 exomes has shown that some variants previously reported to be pathogenic in other disease-related genes have turned out to be harmless later on [28]. As such, newly discovered *GFAP* variants do not guarantee their pathogenicity. This is the reason why researchers resort to functional assays (either in vitro or in vivo) to determine whether novel mutations are pathogenic. In this study, we assessed the pathogenicity of the novel *GFAP* variant p.E138_L148del using in vitro GFAP assembly and sedimentation assays, and GFAP aggregation assays in human SW13 (Vim⁻) cells, rat primary astrocytes and zebrafish embryos. Findings from these studies indicate that the GFAP variant p.E138_L148del is aggregation prone.

To date, 16 GFAP mutations located in the coil 1B segment, including p.E138_L148del, have been found in 26 individuals with type II AxD. To find out the relationship between the AxD subtype and the location of GFAP mutation, approximately 160 pathogenic mutations identified in the GFAP-α transcript (the most common splicing isoform of GFAP) were categorized into two types based on the Prust classification [10], and their distribution at each domain was investigated. As a result, all GFAP mutations in the coil 1B result in type II AxD as opposed to other domains where two subtypes co-exist (Table 2). Furthermore, 13 different in-frame InDel mutations were identified in the whole *GFAP* gene. Among them, all six mutations in the coil 1B showed relatively mild or atypical phenotypes compared with other mutations (Table 1). For example, a previously healthy 32-year-old male with p.R124_L125insQLR mutation presented with spastic quadriparesis of sudden-onset after excessive alcohol consumption [29]. A 9-year-old male with p.R126_L127insRL mutation had abnormal signal change and thickening of the entire SC without atrophy of MO [30], and p.R201del mutation has been reported in a 71-year-old female with progressive left hemiparesis and hemi-hypoesthesia of sudden-onset [31]. Taken together, *GFAP* mutations in the 1B rod domain may be related to Type II AxD, and in-

Table 2. Clinical information of AxD cases with mutations within the 1B rod domain of *GFAP*.

No.	Genetic information			Clinical manifestation										Radiologic manifestation				Ref
	Exon	Codon change	PROVEAN score	Prust	Russo	AAO (Yr)	AAE (Yr)	Bulba	Motor	Urina	Sleep	Scoli	Psych	SPWM	BG	BS	SC	
1	1	p.L123P	−5.829	II	A	45	51	+	+	ND	ND	ND	−	ND	ND	+	−	13
2†	1	p.L123P	−5.829	II	A	50	ND	+	+	ND	ND	ND	−	ND	ND	ND	ND	36
3	1	p.R124_L125insQLR	−8.534	II	A	32	32	+	+	ND	+	ND	+	+	+	+	+	28
4	1	p.R124_L125insE	−7.264	II	A	46	47	+	+	−	−	ND	−	ND	ND	+	+	13
5	1	p.R126_L127insRL	−7.262	II	J	9	ND	+	+	+	ND	+	−	+	−	+	+	29
6	1	p.R126_L127insRL	−7.262	II	A	22	27	+	+	−	−	ND	ND	ND	ND	+	+	13
7	1	p.R126_L127insRL	−7.262	II	A	16	20	−	+	+	+	+	−	+	−	+	+	23
8	1	p.D128N	−3.191	II	A	62	64	−	+	−	−	−	−	−	ND	+	+	38
9	1	p.D128N	−3.191	II	A	68	68	+	+	−	ND	ND	−	−	−	+	+	18
10	1	p.D128N	−3.191	II	A	ND	>52	−	+	ND	ND	−	−	−	−	+	+	39
11	1	p.D128N	−3.191	II	A	64	65	+	+	ND	ND	−	−	+	−	+	ND	40
12*	1	p.E138_L148del	−51.950	II	UD	<20	42	−	+	+	+	+	+	+	+	+	+	*
13	3	p.R201del	−11.288	II	A	71	71	+	+	+	ND	ND	−	ND	ND	+	ND	30
14	3	p.H204R	−6.796	II	A	51	55	+	+	ND	ND	ND	−	−	−	+	+	41
15‡	3	p.E205K	−3.267	II	UD	ND	30	−	−	−	−	−	−	±	ND	+	+	38
16	3	p.E205K	−3.267	II	A	54	58	−	−	+	−	−	−	−	ND	+	+	38
17	3	p.E206K	−3.665	II	A	70	ND	ND	+	+	ND	ND	−	ND	ND	+	ND	42
18	3	p.E206A	−5.486	II	A	40	75	+	+	ND	ND	ND	−	−	−	+	+	43
19	Int.3	p.E207del	−12.417	II	A	ND	76	−	+	−	ND	ND	ND	+	−	+	+	31
20	4	p.E207K	−3.669	II	J	10	ND	+	−	ND	+	−	−	−	+	+	ND	44
21	4	p.E207Q	−2.751	II	J	10	ND	+	−	+	−	+	−	−	+	+	ND	44
22	4	p.E207V	−6.410	II	A	52	52	+	+	ND	ND	−	−	−	−	+	+	45
23	4	p.E210K	−3.403	II	J	4	ND	+	+	+	ND	+	+	±	−	+	ND	29
24	4	p.E210K	−3.403	II	A	24	ND	+	+	ND	+	−	−	+	−	+	ND	9
25	4	p.E210K	−3.403	II	A	58	65	+	+	+	+	+	−	+	ND	+	ND	46
26	4	p.E210K	−3.403	II	J	4	24	+	+	ND	+	+	+	+	ND	+	+	47

*current case; †patient 2 was described to have typical radiologic features consistent with the diagnostic criteria for AxD proposed by van der Knaap with no detailed clinical information; ‡patient 15 presented with chronic headache without neurologic deficits and had a history of analgesic drug abuse.

694

frame InDel mutations of this domain may be associated with mild or atypical presentation.

We conclude that *GFAP* p.E138_L148del is a pathogenic mutation responsible for the development of AxD, and that this case is classified into Prust Type II AxD. Our patient's atypical presentation and clinicoradiologic discrepancy may extend the spectrum of AxD.

DATA AVAILABILITY
The datasets generated and/or analysed during the current study are available from the corresponding author on reasonable request.

REFERENCES
1. Brenner M, Johnson AB, Boespflug-Tanguy O, Rodriguez D, Goldman JE, Messing A. Mutations in GFAP, encoding glial fibrillary acidic protein, are associated with Alexander disease. Nat Genet. 2001;27:117–20.
2. Zang L, Wang J, Jiang Y, Gu Q, Gao Z, Yang Y, et al. Follow-up study of 22 Chinese children with Alexander disease and analysis of parental origin of de novo GFAP mutations. J Hum Genet. 2013;58:183–8.
3. Messing A, Brenner M, Feany MB, Nedergaard M, Goldman JE. Alexander disease. J Neurosci. 2012;32:5017–23.
4. Brenner M, Lampel K, Nakatani Y, Mill J, Banner C, Mearow K, et al. Characterization of human cDNA and genomic clones for glial fibrillary acidic protein. Brain Res Mol Brain Res. 1990;7:277–86.
5. Chernyatina AA, Guzenko D, Strelkov SV. Intermediate filament structure: the bottom-up approach. Curr Opin Cell Biol. 2015;32:65–72.
6. Messing A, Brenner M. GFAP at 50. ASN Neuro. 2020;12:1759091420949680.
7. Srivastava S, Waldman A, Naidu S. Alexander Disease; In: Adam MP, Ardinger HH, Pagon RA, et al. editors: *GeneReviews(®)*. University of Washington, Seattle. 1993.
8. Russo LS Jr, Aron A, Anderson PJ. Alexander's disease: a report and reappraisal. Neurology. 1976;26:607–14.
9. van der Knaap MS, Naidu S, Breiter SN, Blaser S, Stroink H, Springer S, et al. Alexander disease: diagnosis with MR imaging. AJNR Am J Neuroradiol. 2001;22:541–52.
10. Prust M, Wang J, Morizono H, Messing A, Brenner M, Gordon E, et al. GFAP mutations, age at onset, and clinical subtypes in Alexander disease. Neurology. 2011;77:1287–94.
11. Rodriguez D, Gauthier F, Bertini E, Bugiani M, Brenner M, N'Guyen S, et al. Infantile Alexander disease: spectrum of GFAP mutations and genotype-phenotype correlation. Am J Hum Genet. 2001;69:1134–40.
12. Li R, Johnson AB, Salomons G, Goldman JE, Naidu S, Quinlan R, et al. Glial fibrillary acidic protein mutations in infantile, juvenile, and adult forms of Alexander disease. Ann Neurol. 2005;57:310–26.
13. Pedroso JL, Raskin S, Barsottini OG, Oliveira AS. Adult onset Alexander disease presenting with progressive spastic paraplegia. Parkinsonism Relat Disord. 2014;20:241–2.
14. Sawaishi Y. Review of Alexander disease: beyond the classical concept of leukodystrophy. Brain Dev. 2009;31:493–8.
15. Tonduti D, Ardissone A, Ceccherini I, Giaccone G, Farina L, Moroni I. Unusual presentations and intrafamilial phenotypic variability in infantile onset Alexander disease. Neurol Sci. 2016;37:973–7.
16. Yoshida T, Yasuda R, Mizuta I, Nakagawa M, Mizuno T. Quantitative evaluation of brain stem atrophy using magnetic resonance imaging in adult patients with Alexander disease. Eur Neurol. 2017;77:296–302.
17. Shribman S, Reid E, Crosby AH, Houlden H, Warner TT. Hereditary spastic paraplegia: from diagnosis to emerging therapeutic approaches. Lancet Neurol. 2019;18:1136–46.
18. Choi Y, Chan AP. PROVEAN web server: a tool to predict the functional effect of amino acid substitutions and indels. Bioinformatics. 2015;31:2745–7.
19. Der Perng M, Su M, Wen SF, Li R, Gibbon T, Prescott AR, et al. The Alexander disease-causing glial fibrillary acidic protein mutant, R416W, accumulates into Rosenthal fibers by a pathway that involves filament aggregation and the association of alpha B-crystallin and HSP27. Am J Hum Genet. 2006;79:197–213.
20. Nam TS, Kim JH, Chang CH, Yoon W, Jung YS, Kang SY, et al. Identification of a novel nonsense mutation in the rod domain of GFAP that is associated with Alexander disease. Eur J Hum Genet. 2015;23:72–8.
21. Namekawa M, Takiyama Y, Aoki Y, Takayashiki N, Sakoe K, Shimazaki H, et al. Identification of GFAP gene mutation in hereditary adult-onset Alexander's disease. Ann Neurol. 2002;52:779–85.
22. Benzoni C, Aquino D, Di Bella D, Sarto E, Moscatelli M, Pareyson D, et al. Severe worsening of adult-onset Alexander disease after minor head trauma: Report of two patients and review of the literature. J Clin Neurosci. 2020;75:221–3.
23. Liu Y, Zhou H, Wang H, Gong X, Zhou A, Zhao L, et al. Atypical MRI features in familial adult onset Alexander disease: case report. BMC Neurol. 2016;16:211.
24. Sun Y, Wang Z, Li F, Wei L, Sun W, Jin H, et al. A case of adult onset of Alexander disease with nocturnal painless burns, autonomic dysfunction, and peripheral nerve impairment. Clin Neurol Neurosurg. 2021;200:106350.
25. Park J, Park ST, Kim J, Kwon KY. A case report of adult-onset Alexander disease clinically presenting as Parkinson's disease: is the comorbidity associated with genetic susceptibility? BMC Neurol. 2020;20:27.
26. Yasuda R, Nakano M, Yoshida T, Sato R, Adachi H, Tokuda Y, et al. Towards genomic database of Alexander disease to identify variations modifying disease phenotype. Sci Rep. 2019;9:14763.
27. Nishri D, Edvardson S, Lev D, Leshinsky-Silver E, Ben-Sira L, Henneke M, et al. Diagnosis by whole exome sequencing of atypical infantile onset Alexander disease masquerading as a mitochondrial disorder. Eur J Paediatr Neurol. 2014;18:495–501.
28. Lek M, Karczewski KJ, Minikel EV, Samocha KE, Banks E, Fennell T, et al. Analysis of protein-coding genetic variation in 60,706 humans. Nature. 2016;536:285–91.
29. Schmidt H, Kretzschmar B, Lingor P, Pauli S, Schramm P, Otto M, et al. Acute onset of adult Alexander disease. J Neurol Sci. 2013;331:152–4.
30. van der Knaap MS, Ramesh V, Schiffmann R, Blaser S, Kyllerman M, Gholkar A, et al. Alexander disease: ventricular garlands and abnormalities of the medulla and spinal cord. Neurology. 2006;66:494–8.
31. Varanda S, Santos AF, Oliveira TG, Goncalves-Rocha M, Pereira J, Fernandes J, et al. Adult onset leukodystrophy-a possible Alexander's disease. Eur J Neurol. 2015;22:522.

AUTHOR CONTRIBUTIONS
TSN, MDP, and SJL conceived and designed the study. YRK and TSN enrolled the subject and collected clinicoradiologic data. TSN, SJL, YRK, KWK and MKK analyzed and interpreted the clinicoradiologic data. SHL, GC, SYC, MSJ, NHL, AWY and MDP performed functional studies. TSN, MDP and SYC supervised the study. MDP, SYC and TSN wrote the manuscript.

FUNDING

COMPETING INTERESTS
The authors declare no competing interests.

ETHICS APPROVAL
This study was approved by the Institutional Review Board at Chonnam National University Hospital (CNUH-2020-018).

CONSENT FOR PUBLICATION
The patient provided written informed consent for the publication.

ADDITIONAL INFORMATION
Supplementary information The online version contains supplementary material available at https://doi.org/10.1038/s41431-022-01073-2.

Correspondence and requests for materials should be addressed to Ming-Der Perng, Seok-Yong Choi or Tai-Seung Nam.

Reprints and permission information is available at http://www.nature.com/reprints

Publisher's note Springer Nature remains neutral with regard to jurisdictional claims in published maps and institutional affiliations.